

ImputeFormer: Graph Transformers for Generalizable Spatiotemporal Imputation

Tong Nie[§], Guoyang Qin, Yuewen Mei, and Jian Sun*

Abstract—This paper focuses on the multivariate time series imputation problem using deep neural architectures. The ubiquitous issue of missing data in both scientific and engineering tasks necessitates the development of an effective and general imputation model. Leveraging the wisdom and expertise garnered from low-rank imputation methods, we power the canonical Transformers with three key knowledge-driven enhancements, including projected temporal attention, global adaptive graph convolution, and Fourier imputation loss. These task-agnostic inductive biases exploit the inherent structures of incomplete time series, and thus make our model versatile for a variety of imputation problems. We demonstrate its superiority in terms of accuracy, efficiency, and flexibility on heterogeneous datasets, including traffic speed, traffic volume, solar energy, smart metering, and air quality. Comprehensive case studies are performed to further strengthen the interpretability. Promising empirical results provide strong conviction that incorporating time series primitives, such as low-rank properties, can substantially facilitate the development of a generalizable model to approach a wide range of spatiotemporal imputation problems.

Index Terms—Graph Transformers, Data Imputation, Spatiotemporal Modeling, Time Series, Graph Neural Networks.

1 INTRODUCTION

MISSING data is a frequent occurrence in modern detection systems. Sparse observations or measurements pose significant challenges for decision-makers in implementing well-developed, data-driven models for managing and optimizing systems. This issue is particularly prominent in traffic monitoring systems, where the quality of measured data is susceptible to a variety of factors such as adverse weather, energy supply, sensor service time, and light condition [1], [2], [3]. The well-known Performance Measurement System (PeMS) in California, USA [4] suffers from detection errors that cause a large proportion (nearly 40%) of measurements to become invalid or missing.

This issue prompts practitioners to develop advanced models that can fuse available information from limited observations to impute those missing values. To achieve this goal, extensive research has contributed to machine learning methods for application purposes, especially in transportation research [1], [2], [3], [5], [6], [7], [8], [9], [10]. Generally, there exist two research paradigms towards missing data imputation. The first belongs to the low-rank and low-dimensional models, such as [5], [8], [10], [11], [12]. This kind of model typically assumes a well-structured matrix or tensor structure for the data studied. Since the algebraic structures of the matrix or tensor manifold can provide guidance in reconstructing the data [13], it is becoming a simple yet effective method for handling incomplete measurements. However, limited model expressivity hinders

the capture of complex patterns such as nonlinearity and nonstationary, thus being less competitive in reality.

Another dominating direction is deep imputation models. By learning the dynamics of the data-generating process, deep learning-based imputation models have demonstrated great potential and surpass analytical methods [14], [15], [16], [17], [18], [19]. Among these achievements, Transformer-based architectures stand out for their generative output, which can produce imputations more efficiently than autoregressive-based models [17], [18], [20]. Despite the success of neural imputation models on several benchmarks, there are still some remaining problems that need to be fully addressed. First, data-intensive models require a large quantity of observed data to train, and therefore are rendered inadequate in the presence of low-quality training data. Unfortunately, it is challenging for real-world sensor systems to provide a desirable data condition. For example, GPS records in the ride-sharing system are extremely sparse [21]. Second, intricate model structures such as probabilistic diffusion and bidirectional recurrence can consume a substantial amount of computational memory and resources, making them less efficient for real-time deployment. Third, without the guidance of physics or data structures, brute-force training methods are prone to overfit the training data and perform poorly when applied to tasks from different domains or shifted distributions. Therefore, a robust, efficient, and generalizable deep imputation model is needed.

From a technical perspective, these two types of models can complement each other. Matrix- and tensor-based analytical models provide general prior knowledge of spatiotemporal data, such as the low-rank and sparsity nature. While deep learning models have demonstrated impressive representation learning powers. From an application perspective, real-world scenarios prioritize a universal and transferable model capable of approaching various imputation problems, such as coping with cross-domain datasets,

• The authors are with the Department of Traffic Engineering and Key Laboratory of Road and Traffic Engineering, Ministry of Education, Tongji University, Shanghai, China. 201804. E-mail: {nietong, 2015qgy, meiyuewen, sunjian}@tongji.edu.cn.

• Corresponding author: Jian Sun.

• [§]The code will be open-sourced upon publication.

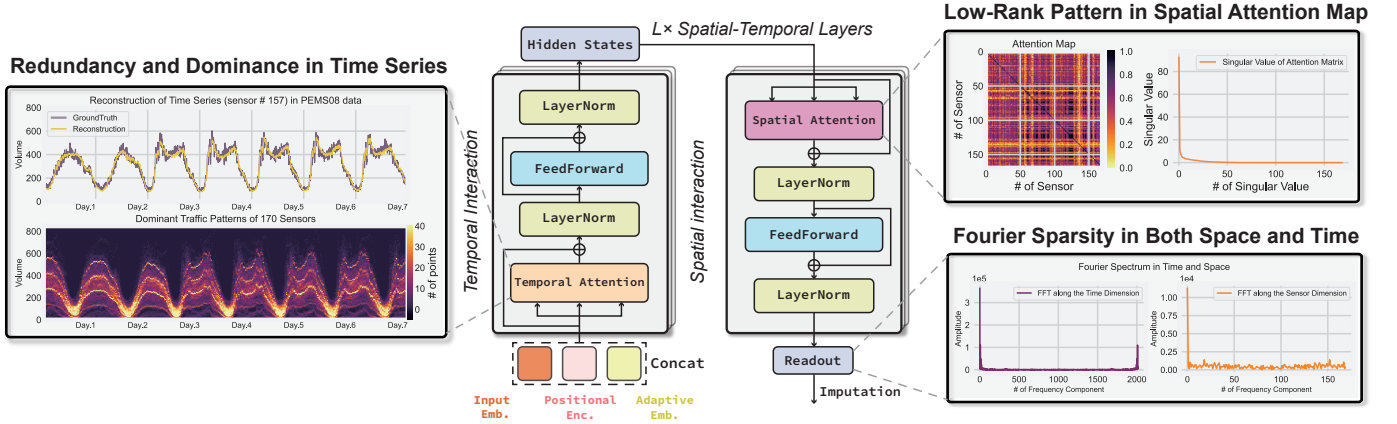


Fig. 1: Illustration on the low-rank nature in time series. (a) Redundancy in time series: there are five dominant traffic patterns in the PEMS08 data that correspond to the five largest singular values, and a reasonable reconstruction of traffic volume can be achieved using only these five singular values. (b) Low-rank pattern in spatial attention map: the singular values of the multivariate correlation (attention) map show a long-tail distribution and most of them are small values. (c) Fourier sparsity in both space and time dimensions: spectral analysis reveals that both the spatial and temporal signals possess a sparse Fourier spectrum, with most amplitudes being close to zero. We exploit these properties as structural biases in temporal and spatial attention modules of ImputeFormer.

varying observation conditions, highly sparse measurements, and different input patterns. How to exploit time-series inductive bias to improve the accuracy, efficiency, and generality of deep imputation models is an open question.

Both methodological and practical limitations encourage us to design an improved and more general model for spatiotemporal imputation. On the one hand, most of existing advanced solutions are evaluated on limited datasets with simple settings, such as traffic speed data with a fixed missing pattern. The effectiveness in a variety of other data types and more challenging imputation scenarios is questioned. On the other hand, although Transformer models tend to have the possibility of becoming foundational architectures for general time series forecasting problem [22], [23], directly applying them to the imputation task can be problematic and cause spurious correlations due to the existence of missing values. Exploration of the potential of Transformers for multivariate time series imputation problems, especially in the context of spatiotemporal data, is still inadequate.

In this paper, we fully exploit the achievements and wisdom of previous low-rank models and enable the knowledge to power the canonical Transformer model (see Fig. 1 for illustration). Graph-based structures and inductive biases related to time series allow our model to efficiently and accurately perform imputation. For brevity, we term our model *Spatiotemporal Imputation Transformers* (ImputeFormer). The methodological and technical contributions are summarized as follows:

- 1) We demonstrate how the low-rank inductive bias can power the Transformers to achieve state-of-the-art imputation performance on spatiotemporal data.
- 2) We showcase its superiority in terms of accuracy, efficiency, and generality in heterogeneous datasets, including traffic, solar, electricity, and air quality.
- 3) Comprehensive case studies and analyses reveal the generality and interpretability of ImputeFormer.

The rest of this article is organized as follows. Section 2 briefly reviews related work on data imputation and specifies the notation. Section 3 details the architecture and modules of ImputeFormer. In Section 4, we evaluate our model on various benchmarks and ablation studies as well as model interpretations are provided. Section 5 concludes this work and provides potential directions.

2 PRELIMINARY AND RELATED WORK

2.1 Notations and Problem Formulations

This section first introduces some notation following the terminology used in previous work [18]. In a sensor network with N static detectors at some measurement positions, spatiotemporal data with context information can be obtained: (1) $\mathbf{X}_{t:t+T} \in \mathbb{R}^{N \times T}$: The observed (incomplete) data matrix containing missing values collected by all sensors over a time interval $\mathcal{T} = \{t, \dots, t+T\}$, where T represents the observation period; (2) $\mathbf{Y}_{t:t+T} \in \mathbb{R}^{N \times T}$: the ground truth (complete) data matrix used for evaluation; (3) $\mathbf{U}_{t:t+T} \in \mathbb{R}^{T \times d_u}$: Exogenous variables describe time series, such as time of day, day of the week, and week of the month information; (4) $\mathbf{V} \in \mathbb{R}^{N \times d_v}$: Sensor-specific meta-information, such as detector ID and location of installation. For ease of representation, this paper uses the terms node, sensor, and location interchangeably.

Given the above elements, the multivariate time series imputation problem is therefore defined as an inductive learning and inference process:

$$\text{Learning } \hat{\Theta} = \arg \min_{\Theta} \sum_{t \in \mathcal{T}} \ell(\text{NN}(\{\mathbf{x}_t, \mathbf{u}_t, \mathbf{m}_t\}, \mathbf{V}|\Theta), \mathbf{x}_t),$$

$$\text{Inference } \hat{\mathbf{x}}_{t'} = \text{NN}(\{\mathbf{x}_{t'}, \mathbf{u}_{t'}, \mathbf{m}_{t'}\}, \mathbf{V}|\hat{\Theta}), \forall \{t' \dots t' + T\}, \quad (1)$$

where $\text{NN}(\cdot|\Theta)$ is the neural network model parameterized by Θ , and the indicator \mathbf{m}_t denotes the locations of the masked values for training and the locations of the observed

values for inference. After training the model on observed data, the imputation model can act on a different time scale from the training set. It is worth mentioning that the ground truth \mathbf{Y} is only used to calculate the evaluation metrics and is not available to the model in this process.

2.2 Related Works

This section provides a review of the literature on the multivariate time series imputation problem. Generally, there exist two series of studies on this topic, including 1) low-dimensional/rank models and 2) neural imputation models. In addition, we discuss existing Transformer-based solutions and techniques for time series self-supervised learning to clarify the connections between our models.

2.2.0.1 Low-Dimensional and Low-Rank Imputation Models: Early methods approached the series data imputation problem by exploring statistical interpolation tools [24], [25]. Recently, low-rank matrix factorization (MF) [12], [26] and low-rank tensor completion models (LRTC) [5], [8], [9], [11], [27] have emerged as numerically efficient techniques for spatiotemporal imputation. To incorporate series-related inductive biases, TRMF [26] imposed autoregressive regularization on the temporal manifold. TiDER [12] decomposed the temporal component into trend, seasonality and bias representations under the MF framework. Despite being conceptually intuitive and concise, the strong assumption about data structure and limited model capacity hinder the real-world efficacy of these low-dimensional models.

2.2.0.2 Neural Imputation Architectures: Recent advancements in neural time series analysis open a new horizon for accurate imputation. Distinct from time series forecasting models, most deep imputation methods either learn to reconstruct the distribution of observed data, or aggregate pointwise information progressively [28]. Representative methods include GRU-D [15], GRUI [29], BRITS [14], GAIN [30], E2GAN [31], NAOMI [32], CSDI [33], PrISTI [19], NRTSI [34]. To harness the multivariate nature of spatiotemporal data, graph neural networks (GNNs) have been adopted to model sensor-wise correlations for more accurate imputation. In particular, MDGCN [35] and GACN [7] applied GNNs with RNNs for traffic data imputation. IGNNK [36], STAR [37], and STCAGCN [38] further tackle the kriging problem, which is a special data imputation scenario. As a state-of-the-art model and a architectural template for GNN-RNN models, GRIN [16] is based on a message passing GRU architecture that progressively performed a two-stage forward and backward recurrent message aggregation. GNNs are employed to encode predefined relational biases.

2.2.0.3 Transformers for Time Series Imputation: Transformers [39] can aggregate abundant information from arbitrary elements within the input, becoming a natural choice for the missing sequential data imputation problem. In particular, CDSA [20] developed a cross-channel self-attention that can utilize correlations in different dimensions. SAITS [17] combined the masked imputation task with an observed reconstruction task, and applied a diagonally-masked self-attention to hierarchically reconstruct the input data. SPIN [18] achieved state-of-the-art imputation performance by conducting a sparse cross-attention and a temporal self-attention on all observed

spatiotemporal points. A two-phase data propagation and a hierarchical loss are also adopted to improve the performance. However, self-attention in the spatial dimension with $\mathcal{O}(N^2)$ (N is the node number) complexity hinders its application in larger graphs.

2.2.0.4 Time Series Masked Modeling: As the data imputation task is basically conditioned on the reconstruction of artificially masked time points or subseries, it seamlessly connects with the time series representation learning problem. Masked time series modeling (MTM) focuses mainly on learning a neural representation for time series by using self-supervised training techniques [40], [41], [42]. Ti-MAE [42] proposed to reconstruct the randomly masked series embedding using a Transformer encoder. PatchTST [41] handled masked patches in long-term series. SimMTM [40] aggregates point-wise information by series-wise similarities. The main difference between time series imputation and representation learning lies in the way missing (masked) values are injected and the training objective. The canonical MTM aims to learn the neural representation that benefits the downstream task, and masking can be done regularly for each series during the training stage. Conversely, series imputation tackles missing values that occurred before training, and the model is optimized to reduce the reconstruction error as much as possible by resorting to the MTM on observed part of the series.

3 GRAPH TRANSFORMERS AS EFFICIENT SPATIOTEMPORAL IMPUTERS

This section elaborates the proposed ImputeFormer model. We first provide an architectural overview of the structure in Section 3.1 and then detail the input embedding design in Sections 3.2 and the spatial-temporal block in Sections 3.3 and 3.4. One distinct difference between our model and other location-aware Transformer models such as Vision Transformers [43] is that our model is permutation invariant but location-aware, which resembles the way of graph convolutional networks (GCNs). But unlike GCNs, ImputeFormer does not require a predefined graph due to the global adaptive interaction between the series, and it also bypasses the use of intricate techniques adopted in recent work such as bidirectional recurrent aggregation, sparse cross-attention, attention masking, and hierarchical loss functions. We provide an illustration to demonstrate the structural difference between ImputeFormer and other architectures in Fig. 2.

3.1 Architectural Overview

The overall structure of the proposed ImputeFormer model is shown in Fig. 1. The input embedding layer transforms sparse observations to hidden states in an additional dimension and incorporates both fixed and learnable embedding into the inputs. Following a Time-and-Graph template [44], TemporalInteraction and SpatialInteraction perform global message passing alternatively on all spatiotemporal coordinates, producing imputed representations of missing points. Finally, a MLP

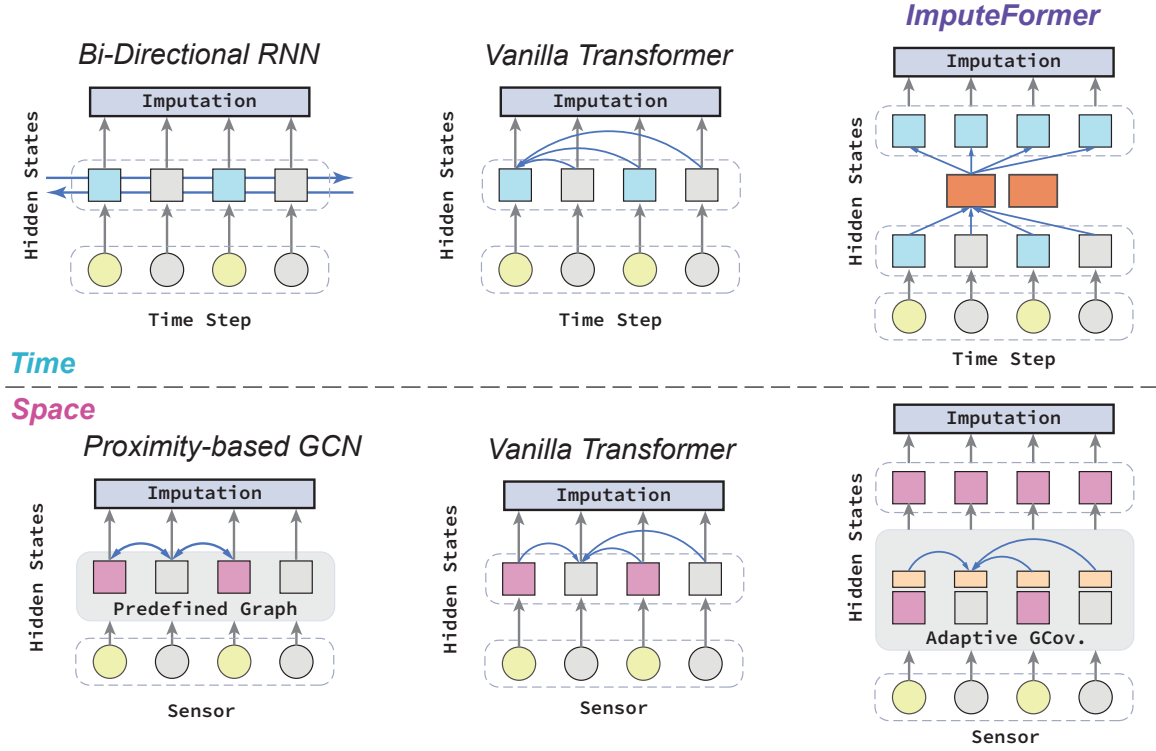


Fig. 2: Architectural comparison of different models. We illustrate how different methods approach the spatial and temporal imputation problem. (a) RNN-GCN model adopts bidirectional RNNs to aggregate available information from consecutive time points and GCN to collect neighborhood information on predefined graphs. (b) Transformer model computes all pairwise correlations of the raw data on both spatial and temporal dimensions. (c) ImputeFormer utilizes projected attention along the temporal axis and global adaptive convolution based on node embedding in the spatial axis.

readout is adopted to output the final imputation. The above process can be summarized as follows.

$$\begin{aligned}
 \mathcal{Z}_{t:t+T}^{(0)} &= \text{InputEmb}(\mathbf{X}_{t:t+T}, \mathbf{U}_{t:t+T}, \mathbf{V}), \\
 \mathcal{Z}_{t:t+T}^{(\ell+1)} &= \text{TemporalInteraction}(\mathcal{Z}_{t:t+T}^{(\ell)}), \\
 \mathcal{Z}_{t:t+T}^{(\ell+1)} &= \text{SpatialInteraction}(\mathcal{Z}_{t:t+T}^{(\ell+1)}), \forall \ell \in \{0, \dots, L\}, \\
 \hat{\mathbf{X}}_{t:t+T} &= \text{Readout}(\mathcal{Z}_{t:t+T}^{(L+1)}).
 \end{aligned} \tag{2}$$

The canonical Transformer block [39] can be adopted in `TemporalInteraction` and `SpatialInteraction` to gather spatial-temporal information for imputation. However, we argue that directly applying self-attention to the imputation problem is questionable. On the one hand, the calculation of pairwise attention is prone to sensitivity toward input data. This results in spurious correlations on top of sparse data that could be misleading. On the other hand, most of the time series are low-rank in nature. Full-attention computation on raw data can be overcorrelated and generate high-rank attention maps and estimations. To address these issues, we start from time series primitives and enhance the Transformer using these priors.

3.2 Spatiotemporal Input Embedding

3.2.0.1 Input Embedding: Unlike images or languages, time series are supposed to have low semantic densities [40], [41]. To exploit this inductive bias, many series forecasting models propose flattening and abstract-

ing the input series to reduce information redundancy [45], [46], [47]. Specifically, given the input multivariate series $\mathbf{X}_{t:t+T} \in \mathbb{R}^{N \times T}$, each series can be represented by a multilayer perceptron (MLP): $\mathbf{z}^{i,(0)} = \text{MLP}(\mathbf{x}^i)$, where $\text{MLP}(\cdot) : \mathbb{R}^T \rightarrow \mathbb{R}^D$ is shared between each series.

However, we argue that this technique can be problematic for series imputation. If we express this mapping as the following expansion:

$$x_{t+h} = \sigma \left(\sum_{k=0}^T w_{k,h} x_{t+k} + b_{k,h} \right), \quad h \in \{0, \dots, T\}, \tag{3}$$

it is evident that the linear weights dependents on the relative position in the sequence and are agnostic to the data flow. Since missing data points and intervals can occur at arbitrary locations in the series, fixed weights can learn spurious relationships between each time step, thus overfitting the missing patterns in the training data.

Therefore, we should avoid using linear mappings on the time axis to account for the varying missing time points. We adopt a dimension expansion strategy [48] to preserve the information density of the input series. In practice, we expand an additional dimension of the input incomplete series and project it into a hidden state along this new dimension:

$$\mathcal{Z}_{t:t+T}^{(0)} = \text{MLP}(\text{Unsqueeze}(\mathbf{X}_{t:t+T}, \text{dim}=-1), \tag{4}$$

where $\text{Unsqueeze}(\cdot) : \mathbb{R}^{N \times T} \rightarrow \mathbb{R}^{N \times T \times 1}$, and $\mathcal{Z}_{t:t+T}^{(0)} \in$

$\mathbb{R}^{N \times T \times D}$ is the initial hidden representation. With this, we can aggregate message from other time points by learning data-dependent weights:

$$\mathbf{Z}_{t:t+T}^{i,(\ell+1)} = \mathcal{F}_\ell(\mathbf{Z}_{t:t+T}^{i,(\ell)}) \mathbf{Z}_{t:t+T}^{i,(\ell)}, \quad (5)$$

where $\mathcal{F}_\ell(\cdot) : \mathbb{R}^{T \times D} \rightarrow \mathbb{R}^{T \times T}$ represents a data-driven function at the ℓ -th layer, such as self-attention.

3.2.0.2 Time Stamp Encoding: Time stamp encoding is adopted to handle the order-agnostic nature of Transformers [39]. As the input series covers a relatively short range, we only consider the time-of-day information. We adopt the sinusoidal positional encoding in [39] to inject the time-of-day information of each time series along time dimension:

$$\begin{aligned} p_{\text{sine}}^t &= \sin(p_t * 2\pi/\delta_D), \\ p_{\text{cosine}}^t &= \cos(p_t * 2\pi/\delta_D), \\ \mathbf{u}_t &= [p_{\text{sine}}^t \| p_{\text{cosine}}^t], \end{aligned} \quad (6)$$

where p_t is the index of t -th time-of-day point in the series, and δ_D is the day-unit time mapping. We concatenate \mathbf{p}_{sine} and $\mathbf{p}_{\text{cosine}}$ as the final time stamp encoding $\mathbf{U}_{t:t+T} \in \mathbb{R}^{T \times 2}$. Note that learnable series encoding is also optional.

3.2.0.3 Spatiotemporal Node Embedding: We consider the use of both predefined and learnable positional encodings as input embeddings for the masked series. Previous work has demonstrated the importance of node identification in distinguishing different sensors for spatiotemporal forecasting problems [45], [46], [49], [50]. Here we also recommend the use of learnable node embedding for imputation task. On the one hand, it benefits the adaptation of local components [49] in graph-based data structure. On the other hand, node embedding can be treated as a low-rank representation (an abstract and compact representation) of the incomplete series, which will be detailed in Section 3.4.

To implement, we can assign each series a random initialized parameter $\mathbf{e}^i \in \mathbb{R}^{D_s}$. We then split the hidden dimension of the static node embedding equally by the length of the time window (we assume that the variable dimension is an integer multiple of the length of the time window) as a *multi-head* node embedding and unfold it to form a low-dimensional and time-varying representation: $\mathbf{E}_{t:t+T}^i \in \mathbb{R}^{T \times D_s/T}$. The implicit interactions between the node embedding, data, and modular components are involved in the end-to-end gradient descent process. Finally, the spatiotemporal input embedding for each node can be formulated as follows:

$$\mathbf{Z}_{t:t+T}^{i,(1)} = \text{Concat}(\mathbf{Z}_{t:t+T}^{i,(0)}; \mathbf{U}_{t:t+T}; \mathbf{E}_{t:t+T}^i, \text{dim}=1), \quad (7)$$

where $\mathbf{Z}_{t:t+T}^{i,(1)} \in \mathbb{R}^{T \times (D+D_s/T+2)}$ is input to the following modules. We will detail each modular design of the spatial-temporal block in the following sections.

3.3 Temporal Interaction with Projected Attention

Self-attention technique has been widely adopted to model temporal relations in both short- and long-term time series forecasting studies [6], [41], [50], [51]. Given a hidden representation $\mathbf{Z}^{i,(\ell)} \in \mathbb{R}^{T \times D'}$ (subscripts are omitted for the sake of brevity), the canonical multi-head self-attention [39]

is computed as follows:

$$\begin{aligned} \tilde{\mathbf{Z}}^{i,(\ell)} &= \text{LayerNorm}(\mathbf{Z}^{i,(\ell)} + \\ &\quad \text{SelfAtten}(\mathbf{Z}^{i,(\ell)}, \mathbf{Z}^{i,(\ell)}, \mathbf{Z}^{i,(\ell)})), \\ \mathbf{Z}^{i,(\ell+1)} &= \text{LayerNorm}(\tilde{\mathbf{Z}}^{i,(\ell)} + \\ &\quad \text{FeedForward}(\tilde{\mathbf{Z}}^{i,(\ell)})), \end{aligned} \quad (8)$$

where $\text{SelfAtten}(\mathbf{Z}, \mathbf{Z}, \mathbf{Z})$ transforms the input into queries $\mathbf{Q} \in \mathbb{R}^{T \times D'}$, keys $\mathbf{K} \in \mathbb{R}^{T \times D'}$, as well as values $\mathbf{V} \in \mathbb{R}^{T \times D'}$, and then outputs a weighted sum of the values according to attention scores as $\text{Softmax}(\mathbf{Q}\mathbf{K}^\top/\sqrt{D'})\mathbf{V}$.

Intuitively, neural representations at unobserved locations can attend to all other observations and obtain a plausible new representation after a series of temporal attentive aggregations. However, after dimension expansion in Eq. (4), there exist varying degrees of redundancy in temporal information. The hidden dimension is typically much larger than the length of the sequence $D' \gg T$, then the pre-Softmax attention score $\mathbb{R}^{T \times D'} \times \mathbb{R}^{D' \times T} \rightarrow \mathbb{R}^{T \times T}$ can be a high-rank matrix. Besides, simply gathering the observations may incur a high cost or lead to potential over-smoothing issues.

As is evident in Fig. 1, time series are supposed to be redundant in the time domain, that is, most of the information can be well reconstructed using only a few modes. Imposing a low-rank constraint on the attentive process of incomplete series can facilitate the reconstruction of hidden spaces. Inspired by the efficient spatial modeling techniques in [51], we propose exploiting a linear complexity projected attention mechanism to efficiently model the pairwise temporal interaction between all available time points in a lower-dimensional space.

To take advantage of the low-rank property as a structural bias for incomplete data [52], we first project the initial features to low-rank representations by attending to a low-dimensional vector. Specifically, we first randomly initialize a learnable vector which is shared by all nodes with the gradient tractable as the *projector* $\mathbf{V}_{\text{proj}} \in \mathbb{R}^{C \times D'}$, where $C \ll T$ is the projected dimension. In order to represent the temporal message in a compact form, we then project the input hidden states to the projected space by attending to the query projector:

$$\begin{aligned} \tilde{\mathbf{Z}}_{\text{proj}}^{i,(\ell)} &= \text{SelfAtten}(\mathbf{V}_{\text{proj}}^{(\ell)}, \mathbf{Z}^{i,(\ell)}, \mathbf{Z}^{i,(\ell)}), \\ &= \text{Softmax}\left(\frac{\mathbf{Q}_{\text{proj}} \mathbf{K}_z^\top}{\sqrt{D'}}\right) \mathbf{V}_z, \end{aligned} \quad (9)$$

where $\tilde{\mathbf{Z}}_{\text{proj}}^{i,(\ell)} \in \mathbb{R}^{C \times D'}$ is the projected value. In particular, since the projector \mathbf{V}_{proj} is decoupled from the spatial dimension, the resulted attention map $\text{Softmax}(\mathbf{Q}_{\text{proj}} \mathbf{K}_z^\top/\sqrt{D'}) \in \mathbb{R}^{C \times T}$ can be interpreted as an indicator of how the incomplete time series can be compressed into a compact representation with shorter length, that is, the low-rank characteristics [8], [11]. More explanations on the projector will be provided in Section 4.8.3.

$\tilde{\mathbf{Z}}_{\text{proj}}^{i,(\ell)}$ stores the principal temporal patterns within the input data. Then, we can recover the complete series with this compact representation by dispersing the projected

information to all other series by serving as a key:

$$\begin{aligned}\hat{\mathbf{Z}}^{i,(\ell)} &= \text{LayerNorm}(\mathbf{Z}^{i,(\ell)} + \\ &\quad \text{SelfAtten}(\mathbf{Z}^{i,(\ell)}, \tilde{\mathbf{Z}}_{\text{proj}}^{i,(\ell)}, \tilde{\mathbf{Z}}_{\text{proj}}^{i,(\ell)})), \\ \mathbf{Z}^{i,(\ell+1)} &= \text{LayerNorm}(\hat{\mathbf{Z}}^{i,(\ell)} + \\ &\quad \text{FeedForward}(\hat{\mathbf{Z}}^{i,(\ell)})),\end{aligned}\quad (10)$$

where $\mathbf{Z}^{i,(\ell+1)} \in \mathbb{R}^{T \times D'}$ is the imputation by the ℓ -th temporal interaction layer. Since the projector in Eqs. (9) and (10) can be obtained by end-to-end learning and is independent of the order in series, it has the property of data-dependent model in Eq. (5).

It should be noted that the “projection-reconstruction” process in Eqs. (9) and (10) resemble the low-rank factorization process [53]. Inflow in Eq. (9) controls the amount of information used to form a dense representation in a lower-dimensional space. Outflow in Eq. (10) determines how hidden states can be reconstructed using a few projected coordinates. Thus, the projected attention is sparse.

This mechanism can also bring about efficiency benefit. The canonical self-attention in Transformers [39] costs $\mathcal{O}(L^2)$ time complexity with the sequence length being L . Although effective in passing messages on all tokens, it is less efficient in long-term series. While the time complexity of the projected attention computation is $\mathcal{O}(T)$, it has the potential for inference on longer sequences. In addition, the above computations can be readily extended to multi-head implementations.

3.4 Spatial Interaction with Global Adaptive Graph Convolution

The availability of observed temporal information of a series is not sufficient for full-scale imputation. For example, temporal models can struggle with out-of-distribution (OOD) imputation of the observed data. This OOD problem is prevalent in traffic data, as traffic congestion can result in unexpected local spatial patterns. Therefore, it is reasonable to exploit the multivariate relationships between series to complement the temporal imputation.

A straightforward way to address this problem is to apply a Transformer block in spatial dimension [7], [50]. Nevertheless, two key concerns prevent the direct use of this technique: (1) *Spurious correlations*: Short-term historical series within a window can be noisy and indistinguishable. Modeling relational structures using pairwise attention or similarity of sparse inputs can generate a high-rank estimation with spurious spatial dependency and redundancy. Such unstable correlations are adverse to the capture of multivariate relationships. On the contrary, the long-term behavior of each series is less sensitive to time-specific events and missing data, and therefore more advantageous to inferring the underlying structures [46], [54], [55]. (2) *High computational cost*: All pairwise attention on large graphs is memory intensive and computationally inefficient for both training and testing in reality.

Consequently, we design a global adaptive graph convolution (GAGC) as an alternative to spatial attention. Recall that the node (sensor) embedding in Eq. (7) not only signifies the identity of each individual but also functions as a low-dimensional abstract of historical series. We then adapt

this endogenous representation for a correlation (attention) map by using the trick of adaptive graph convolutions. Formally, we assume that the message passing happens on a globally connected dense graph, and the graph weights are estimated by the pairwise correlating of node embedding:

$$\begin{aligned}\mathbf{Q}_e^{(\ell)} &= \text{Linear}(\mathbf{E}), \\ \mathbf{K}_e^{(\ell)} &= \text{Linear}(\mathbf{E}), \\ \mathbf{A}^{(\ell)} &= \text{Softmax}\left(\frac{\mathbf{Q}_e^{(\ell)} \mathbf{K}_e^{(\ell)\top}}{\sqrt{D'}}\right),\end{aligned}\quad (11)$$

where $\mathbf{A}^{(\ell)} \in \mathbb{R}^{N \times N}$ denotes the pairwise correlation score of all sensors, and $\mathbf{Q}_e, \mathbf{K}_e \in \mathbb{R}^{N \times D'}$ are linearly projected from the spatiotemporal embedding set $\mathbf{E} = [\bar{\mathbf{e}}^1 \|\bar{\mathbf{e}}^2\| \dots \|\bar{\mathbf{e}}^N] \in \mathbb{R}^{N \times D_s/T}$, where $\bar{\mathbf{e}}^i$ is the static node embedding averaging over the time span (temporal heads) $\{t : t + T\}$ from Eq. (7). Subsequently, Eq. (11) is involved in the global graph convolution process as follows:

$$\begin{aligned}\tilde{\mathbf{Z}}_t^{(\ell)} &= \text{LayerNorm}(\mathbf{Z}_t^{(\ell)} + \mathbf{A}^{(\ell)} \times \mathbf{Z}_t^{(\ell)}), \\ \mathbf{Z}_t^{(\ell+1)} &= \text{LayerNorm}(\tilde{\mathbf{Z}}_t^{(\ell)} + \text{FeedForward}(\tilde{\mathbf{Z}}_t^{(\ell)})),\end{aligned}\quad (12)$$

where $\mathbf{Z}_t^{(\ell+1)} \in \mathbb{R}^{N \times D'}$ is the imputation at step t in the ℓ -th spatial interaction block. Since Eq. (12) is performed independently at each time step, it can be paralleled using the tensor product. Additionally, \mathbf{E} is independent of temporal information and reflects the inherent features of a sensor.

Given the graph representation over a period $\mathcal{Z} \in \mathbb{R}^{N \times T \times D'}$, the time complexity of obtaining a vanilla attention matrix in spatial dimension costs $\mathcal{O}(N^2 T D')$, while the cost of GAGC is $\mathcal{O}(N^2 D')$. Although the overall complexity of GAGC still conditions on the magnitude of spatial dimension, the actual implementation is much faster than the vanilla attention for a long sequence.

More importantly, since \mathbf{E} is decoupled from temporal information, it is robust to missing values and reliable to infer a correlation map for global imputation. The full attention computation on the raw data has the size $\mathbb{R}^{N \times (T \times D')} \times \mathbb{R}^{(T \times D') \times N} \rightarrow \mathbb{R}^{N \times N}$, while the GAGC attention has $\mathbb{R}^{N \times D'} \times \mathbb{R}^{D' \times N} \rightarrow \mathbb{R}^{N \times N}$. In this sense, the attention map in Eq. (11) is obtained by the low-dimensional abstract of the input data, acting as a low-rank factorized approximation of full attention.

3.5 Fourier Imputation Loss and Training Strategy

We design several task-specific learning strategies to achieve effective training and generalization of imputation models.

First, to evaluate the model, we simulate different observation conditions by removing parts of the raw data to construct incomplete samples based on different missing rates (p_{missing}). The evaluation metrics are then calculated on these simulated missing points. We use a masking indicator $\mathbf{M}_{\text{missing}}$ to denote these locations in which the unobserved (missing) values are marked as 1, observed as 0.

Second, one salient feature of an imputation model is the design of the loss function. Previous studies proposed adopting accumulated and hierarchical loss [16], [17], [18] to improve the supervision of layerwise imputation. However, we argue that hierarchical loss is not necessary and may generate a biased model as well as over-fitting. Instead, we

Algorithm 1 ImputeFormer - Forward Workflow.

Require: Incomplete time series $\mathbf{X} \in \mathbb{R}^{N \times T}$; input length T ; sensor number N ; spatiotemporal embedding size D_{emb} ; input embedding size D_{in} ; number of spatiotemporal layers L ; masking probability p_{whiten} ; projected dimension size C .

- 1: $\mathbf{X}_{t:t+T} = \text{Mask}(\mathbf{X}_{t:t+T}, p_{\text{whiten}})$ ▷ Training masking with p_{whiten} .
- 2: ▷ Initialize the spatiotemporal embedding.
- 3: $\mathbf{E}_{t:t+T}^i = \text{Parameter}(T, D_{\text{emb}})$, $i = \{1, \dots, N\}$ ▷ $\mathbf{E}_{t:t+T}^i \in \mathbb{R}^{T \times D_{\text{emb}}}$
- 4: ▷ Expand the last dimension to get the initial state.
- 5: $\mathbf{Z}_{t:t+T}^{(0)} = \text{MLP}(\text{Unsqueeze}(\mathbf{X}_{t:t+T}, \text{dim}=-1))$ ▷ $\mathbf{Z}_{t:t+T}^{(0)} \in \mathbb{R}^{N \times T \times D_{\text{in}}}$
- 6: ▷ Spatiotemporal input embedding.
- 7: $\mathbf{Z}_{t:t+T}^{i,(1)} = \text{Concat}(\mathbf{Z}_{t:t+T}^{i,(0)}; \mathbf{U}_{t:t+T}; \mathbf{E}_{t:t+T}^i, \text{dim}=-1)$, $i = \{1, \dots, N\}$ ▷ $\mathbf{Z}_{t:t+T}^{i,(1)} \in \mathbb{R}^{N \times T \times D'}$
- 8: **for** ℓ **in** $\{2, \dots, L\}$: ▷ Run through ImputeFormer blocks.
- 9: ▷ Projected attention is applied in the time dimension for temporal imputation.
- 10: $\mathbf{Z}_{t:t+T}^{i,(\ell-1)} = \text{TemporalInteraction}(\mathbf{Z}_{t:t+T}^{i,(\ell-1)}, \mathbf{V}_{\text{proj}})$, $i = \{1, \dots, N\}$ ▷ $\mathbf{Z}_{t:t+T}^{i,(\ell-1)} \in \mathbb{R}^{T \times D'}$, $\mathbf{V}_{\text{proj}} \in \mathbb{R}^{C \times D'}$
- 11: ▷ Global adaptive graph convolution is applied in the space dimension for spatial imputation.
- 12: $\mathbf{Z}_t^{(\ell)} = \text{SpatialInteraction}(\mathbf{Z}_t^{(\ell-1)}, \mathbf{E}_t)$, $t = [t, \dots, t+T]$ ▷ $\mathbf{Z}_t^{(\ell)} \in \mathbb{R}^{N \times D'}$, $\mathbf{E}_t \in \mathbb{R}^{N \times D_{\text{emb}}}$
- 13: **End for**
- 14: ▷ Readout and dimension reduction layer.
- 15: $\hat{\mathbf{X}}_{t:t+T} = \text{Squeeze}(\text{MLP}(\mathbf{Z}^L))$ ▷ $\hat{\mathbf{X}}_{t:t+T} \in \mathbb{R}^{N \times T}$
- 16: **Return** $\hat{\mathbf{X}}_{t:t+T}$ ▷ Return the final imputation result $\hat{\mathbf{X}}_{t:t+T}$.

propose a new Fourier imputation loss (FIL) as an inductive bias for the time series imputation task.

As discussed above, spatiotemporal data such as traffic data usually features a low-rank property in the time domain [5], [8], [9], which has been shown to be equivalent to a sparsity in the spectral domain [56]. In other words, we can obtain a reasonable imputation by constraining the rank of the estimated spatiotemporal tensor in the time domain or the sparsity of Fourier coefficient in the frequency domain. Moreover, as the spatiotemporal matrix can be regarded as a special RGB image from a global viewpoint, it also features a sparse Fourier spectrum in the space dimension [56].

However, directly optimizing the rank of the tensor or matrix is challenging [52], as it includes some nontrivial or nondifferentiable computations such as truncated singular value decomposition. Considering the above equivalence, we instead achieve this goal in the frequency domain:

$$\begin{aligned} \bar{\mathbf{X}} &= \mathbf{M}_{\text{missing}} \odot \hat{\mathbf{X}} + (1 - \mathbf{M}_{\text{missing}}) \odot \mathbf{Y}, \\ \mathcal{L}_{\text{FIL}} &= \frac{1}{NT} \sum |\text{Flatten}(\text{FFT}(\bar{\mathbf{X}}, \text{dim} = [0, 1]))|, \end{aligned} \quad (13)$$

where $\text{FFT}(\cdot)$ is the Fast Fourier Transform (FFT), $\text{Flatten}(\cdot) : \mathbb{R}^{N \times T} \rightarrow \mathbb{R}^{NT}$ rearranges the tensor form and $|\cdot|$ is the vector ℓ_1 norm. We apply the FFT on both the space and time axes and then flatten it into a long vector. \mathcal{L}_{FIL} is in fact a unsupervised loss that encourages the imputed values to be naturally compatible with the observed values globally. Note that the ℓ_1 norm computes the mode of the complex vector, ensuring the operation in the real domain.

Lastly, an effective supervised training scheme is needed. During model training, we further randomly whiten a proportion of incomplete observations (p_{whiten}) to create supervised samples. This operation ensures the generalizability of the imputation model (see Section 4.7.2). We use a masking indicator $\mathbf{M}_{\text{whiten}}$ to denote these locations in which the masked values are marked as 1, others as 0. Note that the

reconstruction (supervision) loss is only calculated on these manually whitened points, and models are forbidden to have access to the masked missing points used for evaluation (i.e. $\mathbf{M}_{\text{missing}}$). Therefore, the reconstruction loss of our model is a straightforward ℓ_1 loss on the output of the final readout layer:

$$\mathcal{L}_{\text{recon}} = \frac{1}{NT} \sum |\mathbf{M}_{\text{whiten}} \odot (\hat{\mathbf{X}} - \mathbf{Y})|. \quad (14)$$

Finally, the total loss function is formulated as:

$$\mathcal{L} = \mathcal{L}_{\text{recon}} + \lambda \mathcal{L}_{\text{FIL}}, \quad (15)$$

where λ is a weight hyperparameter. It is worth commenting that the two loss functions complement each other: $\mathcal{L}_{\text{recon}}$ prompts the model to reconstruct the masked observations as precisely as possible in the space-time domain and \mathcal{L}_{FIL} powers the model to generalize on unobserved points in the spectral domain. This makes ImputeFormer works effectively on highly sparse observations.

In summary, the complete forward workflow of ImputeFormer is briefly presented in Algorithm 1.

4 EMPIRICAL EVALUATIONS

In this section, we benchmark the proposed model on several well-known traffic flow datasets, comparing it with state-of-the-art baselines, as well as evaluating its generality to other data sources and different tasks. Then comprehensive analysis and model interpretations are provided.

4.1 Datasets and Experimental Settings

4.1.0.1 Traffic Speed Data: Our experiments include two commonly used traffic speed datasets, named METR-LA and PEMS-BAY. METR-LA contains spot speed data from 207 loop sensors over a period of 4 months from Mar 2012 to Jun 2012, located at the Los Angeles County highway network.

TABLE 1: Results on PEMS-BAY and METR-LA benchmarks.

Models	Point missing		Block missing	
	PEMS-BAY	METR-LA	PEMS-BAY	METR-LA
Average	5.45	7.52	5.48	7.43
MICE [24]	2.82	2.89	2.36	2.73
TRMF [26]	2.10	3.51	2.09	3.36
LRTC-AR [11]	0.94	2.14	4.05	5.35
Bi-MPGRU	0.72	2.00	1.41	2.33
rGAIN [30]	1.90	2.81	2.21	2.95
BRITS [14]	1.84	2.42	1.91	2.40
SAITS [17]	1.33	2.25	1.58	2.32
Transformer [39]	0.76	2.18	1.69	3.58
ST-Transformer	0.75	2.19	1.71	3.58
TIDER [12]	1.43	2.68	2.46	4.95
TimesNet [57]	1.47	2.93	2.73	4.79
GRIN [16]	0.68	1.91	1.20	2.08
SPIN [18]	0.79	1.93	1.13	2.02
ImputeFormer	0.64	1.81	0.95	1.86

PEMS-BAY records 6 months of speed data from 325 static detectors in the San Francisco South Bay Area.

4.1.0.2 Traffic Volume Data: There are four traffic volume datasets to evaluate our model, including PEMS03, PEMS04, PEMS07, and PEMS08. PEMS0X contains the real-time highway traffic volume information in California, which is collected by the Caltrans Performance Measurement System (PeMS) [4] in every 30 seconds. The raw traffic flow is aggregated into 5-minute interval for experiments. Similar to METR-LA and PEMS-BAY, PEMS0X also includes a adjacency graph calculated by the physical distance between sensors.

4.1.0.3 Additional Datasets: Two additional datasets are selected to evaluate the generality of models, including: (1) *Solar*: solar power production records from 137 synthetic PV farms in Alabama state in the year 2006, which are sampled every 10 minutes; (2) *CER-EN*: smart meters measuring energy consumption from the Irish Commission for Energy Regulation Smart Metering Project [58]. Following the setting in [16], we select 435 time series aggregated at 30 minutes for evaluation. (3) *AQI*: PM2.5 pollutant measurements collected by 437 air quality monitoring stations in 43 Chinese cities from May 2014 to April 2015 with the aggregation interval of 1 hour. Note that raw AQI data contains nearly 26% missing data.

4.1.0.4 Missing patterns: For traffic, solar and CER-EN data, we consider two scenarios discussed in [16], [18]: (1) point missing: randomly remove observation points with 25% probability; (2) block missing: randomly drop 5% of the available data and at the same time simulate a sensor failure lasting for $\mathcal{L} \sim \mathcal{U}(12, 48)$ steps with 0.15% probability. We keep the above missing rates the same as in the previous works [16], [18] to benchmark our model. For supplementary experiments, we also evaluated the performance under sparser conditions. For example, the block missing with 10% probability corresponds to a total missing rate of $\approx 90 \sim 95\%$ in our case. Note that matrix or tensor models can only handle in-sample imputation, where the observed training data and the evaluating data are in the same time period. Whereas, deep imputation models can work in an out-of-sample scenario where the training and evaluating

sequences are disjoint. In our experiments, we adopt the out-of-sample routine for deep imputation models and in-sample manner for other models.

4.1.0.5 Baseline Methods: We compare our model with both state-of-the-art and classic methods in related literature. For statistical and optimization models, we consider: (1) Observation average (Average); (2) Temporal regularized matrix factorization (TRMF) [26]; (3) Low-rank autoregressive tensor completion (LRTC-AR) [11]; (4) MICE [24]. For deep imputation models, we select several competitive baselines: (1) SPIN [18]: sparse spatiotemporal attention model with state-of-the-art imputation performance; (2) GRIN [16] message-passing-based bidirectional RNN model with competitive performance; (3) SAITS [17]: Temporal Transformer model with diagonally masked attention; (4) BRITS [14]: bidirectional RNN model for imputation; (5) rGAIN [30]: GAIN model with bidirectional recurrent encoder and decoder; (6) Transformer/ST-Transformer [39]: canonical Transformer model with self-attention in temporal or spatial-temporal dimensions; (7) TiDER [12]: matrix factorization with disentangled neural representations; (8) TimesNet [57]: 2D convolution-based general time series analysis model; (9) BiMPGRU: a bidirectional RNN based GCN model which is similar to DCRNN [59].

4.2 Model Implementations

We build our model and other baselines based on the SPIN repository¹ using PyTorch. All experiments are conducted on a single NVIDIA RTX A6000 (48 GB) GPU. For the hyperparameters of ImputeFormer, we set the hidden size at 256, the input projection size to 32, the node embedding size to 96, the projected size to 8, and the number of spatiotemporal layers to 3. The settings of other baselines can refer to the SPIN repository or our open-source implementations.

4.3 Results on Traffic Benchmarks

The imputation results on traffic speed and volume data are given in Tab. 1 and 2. As can be seen, ImputeFormer consistently achieves the best imputation accuracy on all traffic benchmarks. Two strong competitors GRIN and SPIN show promising results on traffic speed datasets, which are align with the results of their respective papers. However, their performances are inferior on volume datasets, and are surpassed by simple baselines such as ST-Transformer and Bi-MPGRU. Compared to deep imputation models, pure low-rank methods such as matrix factorization and tensor completion models are less effective due to limited model capacity. As for missing patterns, the structured block missing pattern is more challenging than the point missing case. For instance, the vanilla Transformer solution is competitive in point missing case, while is ineffective in block missing case. Nevertheless, ImputeFormer outperforms other baselines by a large margin in this tricky scenario.

4.4 Results on Other Benchmarks

By exploiting the underlying low-rank structures, ImputeFormer can serve as a general missing data

1. <https://github.com/Graph-Machine-Learning-Group/spin>

TABLE 2: Results on PEMS03, PEMS04, PEMS07 and PEMS08 benchmarks.

Models	Point missing				Block missing			
	PEMS03	PEMS04	PEMS07	PEMS08	PEMS03	PEMS04	PEMS07	PEMS08
Average	85.30	103.61	122.35	89.51	85.56	103.82	123.05	89.42
MICE	20.07	28.60	37.11	30.26	21.90	32.45	37.20	26.66
TRMF	18.80	24.34	29.06	20.27	18.71	24.47	29.42	19.80
Bi-MPGRU	11.23	15.84	15.66	11.90	13.87	19.81	21.12	15.89
rGAIN	13.32	22.86	24.41	16.33	14.85	23.26	26.69	27.12
BRITS	12.74	20.00	23.97	15.78	12.01	19.80	23.26	16.37
SAITS	12.40	20.23	22.81	15.12	12.27	20.35	22.82	16.80
Transformer	12.04	16.76	16.86	12.58	24.07	29.63	33.14	25.61
ST-Transformer	11.44	16.22	15.84	11.19	23.55	29.17	32.14	24.67
TimesNet	14.99	20.40	22.00	16.53	44.85	51.05	60.90	45.78
GRIN	10.31	16.25	11.90	12.33	12.28	23.23	16.04	19.69
SPIN	12.85	18.96	17.61	15.02	14.68	19.85	16.99	16.81
ImputeFormer	8.47	14.92	11.68	11.06	9.02	16.83	14.07	12.68

estimator in a variety of spatiotemporal tasks. To demonstrate the versatility of the proposed architecture, we perform experiments on other data sources. Specifically, we evaluate our model on datasets with missing observations and without predefined graphs. Results are given in Tab. 3.

It is observed that `ImputeFormer` also exhibits superiority in other spatiotemporal datasets beyond traffic data. In particular, the correlation of solar stations cannot be described by physical distance and can be inferred from the data. However, after comparing the performance of `Transformer`, `ST-Transformer`, `SAITS`, and `ImputeFormer`, it can be concluded that direct attention computations on both temporal and spatial dimensions are less beneficial than low-rank attention in `ImputeFormer`. Furthermore, the spatial correlation of energy production is less pronounced. The canonical attention on the spatial axis can be redundant and generate spurious correlations. Instead, the use of GAGC can alleviate this issue to some extent.

4.5 Ablation study

To justify the rationale of model designs, we conduct ablation studies on the model structure. Particularly, we examine the following three aspects of `ImputeFormer`:

- 1) Temporal blocks: we replace the temporal interaction module with MLP or directly remove it;
- 2) Spatial blocks: we replace the spatial interaction module with MLP or directly remove it;
- 3) Loss function: We remove the FIL or replace it with a hierarchical loss used in [17], [18].

We adopt the PEMS08 and METR-LA datasets to evaluate each variation. And other experimental settings are consistent with section 4.3. Results are shown in Tab. 4. Several intriguing findings can be observed in this table: (1) After removing any of the attention module along the space and time axis, the performance degenerates substantially; Especially, the spatial interaction module contributes to the inference of block missing patterns significantly, while the temporal modules are crucial for point missing scenarios. (2) The incorporation of MLP benefits little for the imputation, which validates our argument in section 3.2. (3) Compared

to hierarchical loss on the supervised points, FIL generalizes on the unobserved points and effectively reduce the estimation errors.

4.6 Model efficiency

Demonstrating high efficiency in the class of Transformers and RNNs models is also a significant superiority of `ImputeFormer`. We therefore evaluate the efficiency of different architectures. To give a unbiased comparison, we set the batch size to 32 and the hidden size to 128 for all models. Results are shown in Fig. 3. Intuitively, it can be seen that `ImputeFormer` exhibits high training efficiency. Thanks to the low-rank design philosophy, our architecture is approximately 15 times faster than state-of-the-art Transformer baseline (SPIN). It is also cost-effective in GPU memory consumption.

4.7 Further Discussions

To help better understand the superiority of `ImputeFormer` and demonstrate its generality, this section provides more discussions and analysis, including training techniques, different inference scenarios, and case studies.

4.7.1 Random masking in training

The random masking strategy is utilized to create supervision samples for model training. Therefore, the distribution of masking samples of training data and missing observations of testing data should be close to ensure good performance, which is recognized in our previous work [38]. However, it can be difficult to know exactly the missing patterns or missing rates in advance in many real-world scenarios. Therefore, a proper masking strategy is of vital importance. To evaluate the impact of the masking rate in training data, we further consider four different masking strategies during model training: the masking rates are set to 0.25, 0.5, 0.75, and a combination of them [0.25, 0.5, 0.75] respectively. We use the PEMS03 data as a demonstration. Results are shown in Tabs. 5 and 6.

As expected, most models perform best when the masking rate is close to the missing rate in the point missing scenario (e.g., 25%). However, when the missing rate is unclear

TABLE 3: Results on AQI and Solar benchmarks. For Solar data, we compare the performances of baselines that are independent of the predefined graphs.

Models	SOLAR		CER-EN		Simulated faults	
	Point Missing	Block Missing	Point Missing	Block Missing	AQI-36	AQI
Average	7.60	7.56	0.583	0.596	61.81	43.78
MICE	1.59	1.58	0.535	0.555	38.90	29.12
TRMF	2.44	2.35	0.557	0.559	41.91	27.67
Bi-MPGRU	N.A.	N.A.	0.247	0.327	12.02	15.41
rGAIN	1.52	1.64	0.418	0.440	15.69	22.13
BRITS	1.28	1.34	0.351	0.366	14.74	20.72
SAITS	0.98	1.25	0.341	0.368	19.79	21.09
Transformer	2.19	3.58	0.254	0.353	14.99	17.04
ST-Transformer	2.17	3.57	0.251	0.351	13.27	18.55
TIDER	2.84	3.87	0.336	0.377	32.85	18.11
TimesNet	2.93	4.73	0.328	0.460	32.30	28.99
GRIN	N.A.	N.A.	0.235	0.341	12.08	14.51
SPIN	N.A.	N.A.	OOM	OOM	11.89	14.31
ImputeFormer	0.51	0.89	0.239	0.299	11.67	13.40

TABLE 4: Ablations on ImputeFormer. We remove or replace specific components and report corresponding results.

Variation	Component		PEMS08		METR-LA	
	Spatial	Temporal	Point	Block	Point	Block
ImputeFormer	Attention	Attention	11.24	12.86	1.80	1.88
Replace	Attention	MLP	16.95	17.11	2.39	2.28
	MLP	Attention	12.84	17.42	2.20	2.92
	MLP	MLP	34.72	34.41	5.80	5.79
w/o	Attention	w/o	17.06	17.13	2.39	2.28
	w/o	Attention	12.87	17.44	2.21	2.93
Loss function	w/o FIL		11.37	12.97	1.85	1.93
	Hierarchical loss		11.35	13.07	1.84	1.92

TABLE 5: Results on PEMS03 data (25% point missing) with various masking strategies.

Models	Masking Probability			
	25%	50%	75%	Combination
Bi-MPGRU	11.30	11.52	12.20	11.48
BRITS	13.06	13.86	16.06	13.70
SAITS	12.42	16.13	21.63	12.61
ST-Transformer	11.19	11.43	12.22	11.39
GRIN	9.55	9.74	10.39	9.72
SPIN	11.08	11.21	13.85	12.04
ImputeFormer	7.66	8.16	11.44	8.45

TABLE 6: Results on PEMS03 data (block missing) with various masking strategies.

Models	Masking Probability			
	25%	50%	75%	Combination
Bi-MPGRU	13.32	13.36	13.96	13.33
BRITS	12.26	13.01	15.58	12.63
SAITS	12.35	15.73	20.14	12.32
ST-Transformer	23.51	23.76	23.90	23.26
GRIN	11.94	12.05	12.68	11.99
SPIN	13.10	13.68	13.84	13.97
ImputeFormer	8.89	9.23	16.96	8.80

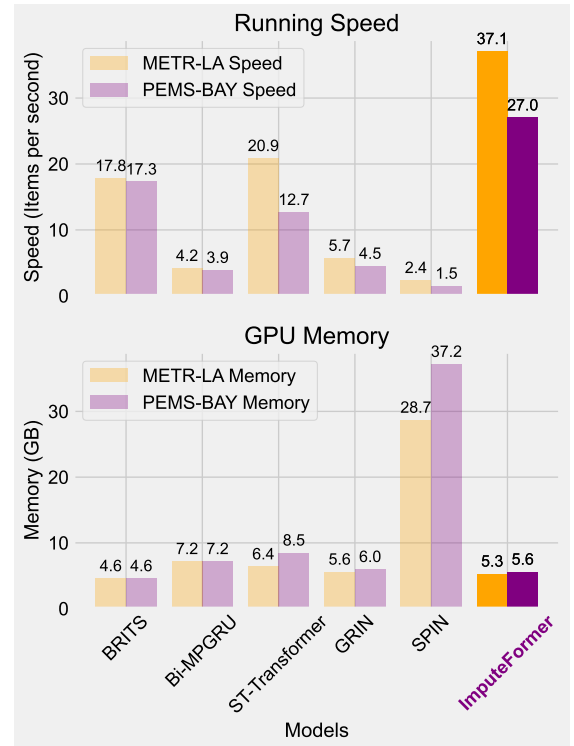


Fig. 3: Comparison of computational efficiency.

due to randomness within the failure generation process, such as the block missing pattern, the combination strategy is more advantageous. For example, Transformer-like model including ST-Transformer, SAITS, and ImputeFormer can benefit from this strategy. More importantly, such a hybrid masking method enables the model to work successfully on varying observation rates during inference.

4.7.2 Inference under different missing rates

Deep imputation models are subject to the distribution shift problem between training and testing datasets. A desirable characteristic is that a model can deal with different missing patterns during inference. Therefore, we consider

a challenging scenario in which a model is trained with a fixed missing rate, but evaluated on different scenarios with varying missing rates. This is, in fact, a zero-shot transfer evaluation. Results are given in Tabs. 7. It is noteworthy that both `ImputeFormer` and `SPIN` are more robust than other baselines in these scenarios. The RNNs and vanilla Transformer models can overfit the training data with a fixed data missing pattern, thereby showing inferior generalization ability.

TABLE 7: Inference under varying missing rate with a single trained model (Zero-shot).

Models	PEMS08			METR-LA		
	Missing rate			Missing rate		
	50%	75%	95%	50%	75%	95%
BRITS	17.21	22.01	52.78	2.61	3.04	5.11
SAITS	16.03	31.32	83.79	2.44	3.37	6.80
ST-Transformer	11.65	13.11	39.95	2.32	2.72	5.16
GRIN	13.25	16.06	42.61	2.06	2.39	4.07
SPIN	15.13	15.51	18.30	2.11	2.34	3.03
ImputeFormer	11.52	12.18	17.35	1.96	2.17	2.79

4.7.3 Inference with varying sequence length

In reality, the imputation model can confront with time series with different length and sampling frequency. As the Transformer model has the ability to work on inputs with different sequence lengths, we can adopt a well-trained model to perform inference on varying sequence length. Results are shown in Fig. 4. It is obvious that `ImputeFormer` can readily generalize to input sequences with different lengths.

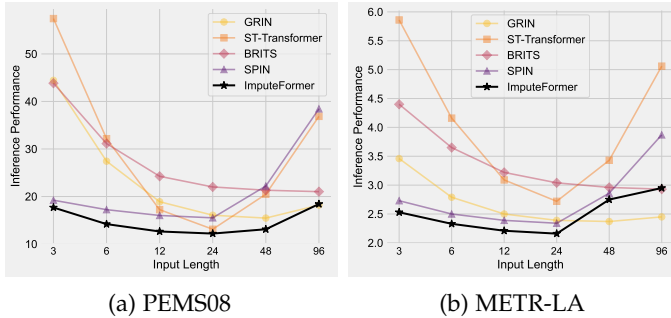


Fig. 4: Inference under different lengths of input sequence with a single trained model (zero-shot).

4.7.4 Dealing with highly sparse observation

To evaluate the performance of our method on highly sparse data, we further train and test `ImputeFormer` on scenarios with lower observation rates. Results are shown in Tab. 8.

Generally speaking, both Transformer- and RNN-based architectures are susceptible to sparse training data. Due to the low-rank constraints on both neural representations and the loss function, `ImputeFormer` is relatively more robust with highly sparse data. Since the attention matrices in `SPIN` are calculated only on observed points, it is more stable than other baselines. But our model consistently achieves lower imputation errors.

TABLE 8: Results on PEMS08 data (point missing) with sparse observations (Training from scratch).

Models	Missing rate			
	60%	70%	80%	90%
BRITS	18.60	19.75	21.44	24.17
SAITS	17.53	18.24	19.39	21.27
ST-Transformer	13.67	14.32	15.86	23.98
GRIN	14.04	15.01	17.26	25.47
SPIN	13.64	14.30	15.19	17.13
ImputeFormer	12.57	13.17	13.98	15.94

4.8 Case Studies

To enhance the interpretability of `ImputeFormer`, we provide several case studies to discuss the functionality of spatial-temporal interaction blocks and visualizations of imputation results.

4.8.1 Imputation visualization

We provide several visualization examples of the traffic datasets studied in Fig. 5. As evidenced by Fig. 5, `ImputeFormer` can generate reasonable estimations for missing values by learning the inherent structures of multivariate time series. Previous studies have discovered that low-rank imputation models can cause oversmoothing estimation [9], [11]. Due to the representation power of deep architecture, our model can provide a detailed reconstruction. In particular, although only limited temporal information is available for reference in the block missing case, the model can resort to the node embedding as the query to spatial relations.

4.8.2 Explanations on spatial embedding

As stated above, the node embedding serves as a compact representation of the incomplete signal of a series (sensor). We use an implicit learning trick to obtain this embedding. Fig. 6 (a) displays the t-SNE visualization of each node embedding with two projected coordinates. The embeddings tend to form clusters, and different clusters are apart from others. This phenomenon is in accordance with highway traffic sensor systems that proximal sensors share similar readings within a time period. From another perspective, we analyze the singular value spectrum of the PEMS08 data in Fig. 6 (b). The incomplete data shows a significant low-rank property, but the singular values of corrupted data dramatically expand. In contrast, the learnable node embedding also obeys a similar low-rank distribution, which can act as a dense surrogate for each sensor.

Taking it a step further, we analyze the multivariate attention map obtained by correlating the node embedding in Fig. 7. To obtain a referable correlation map of complete data, we calculate the absolute value of Pearson coefficient in Fig. 7 (c). It is evident that as the GAGC layers become deeper, the learned attention maps approach the actual ones. Nevertheless, the incomplete data produce noisy correlations with little useful information.

4.8.3 Explanations on temporal projector

Recall that we design the temporal projector to reduce redundancy in the representation of incomplete series. By

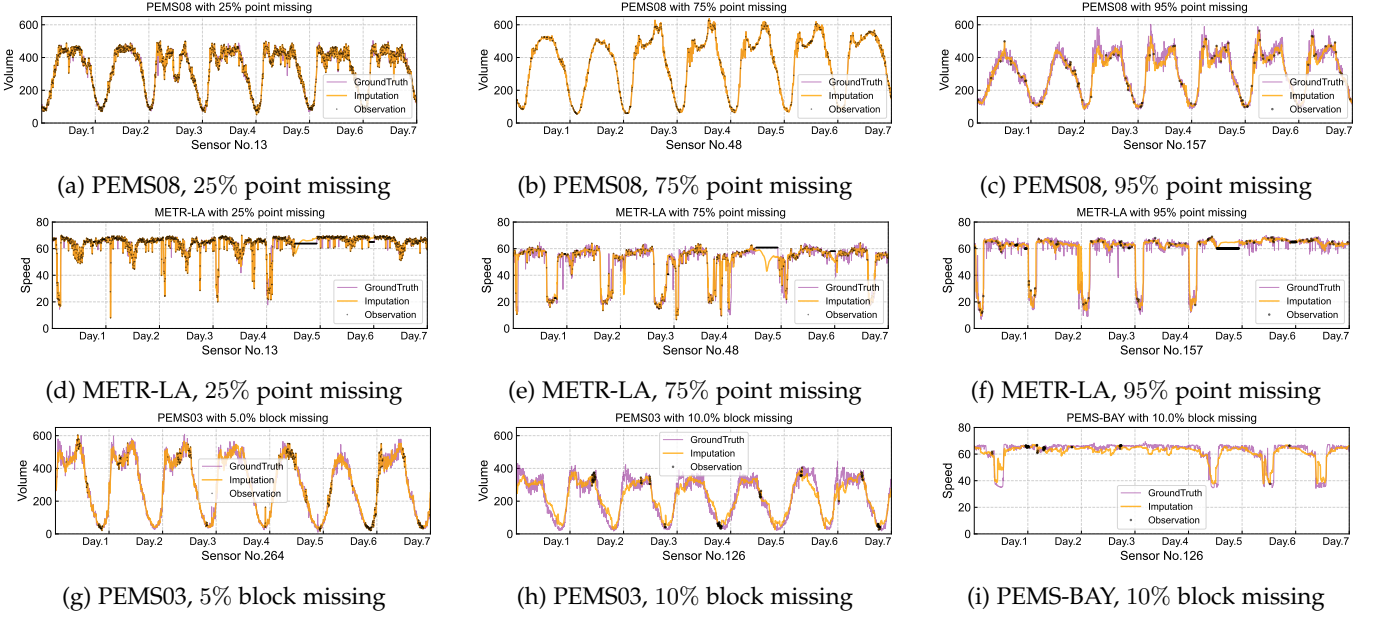


Fig. 5: Visualization examples of imputation for traffic speed and volume data under different missing patterns.

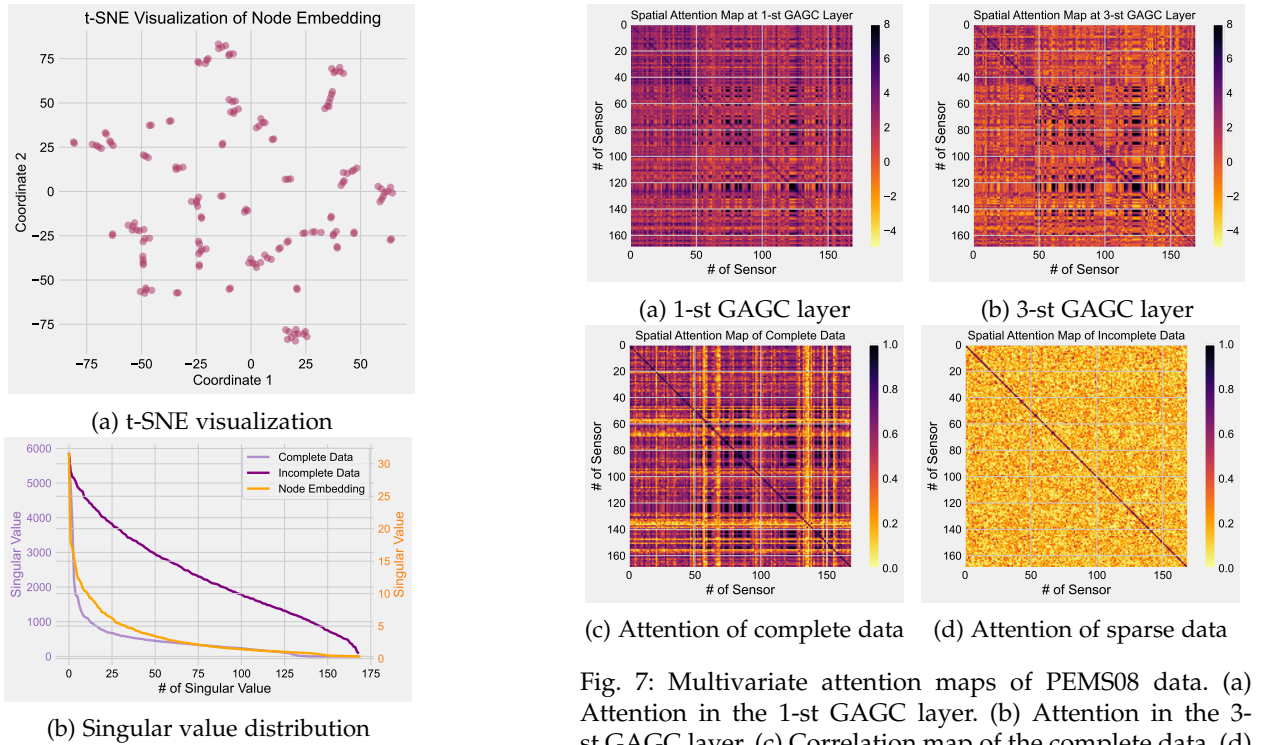


Fig. 6: Explanations on node (sensor) embedding using PEMS08 data. (a) Two-dimensional t-SNE visualization of each node embedding. (b) Singular spectrum of complete data, incomplete observations, and node embedding.

projecting the whole series into a compact representation, the projected attention in Eqs. (9) and (10) can filter effective information for reconstruction. To illustrate this process, we display the inflow and outflow attention maps in Figs. 8 and 9.

It can be observed that these matrices quantify how

Fig. 7: Multivariate attention maps of PEMS08 data. (a) Attention in the 1-st GAGC layer. (b) Attention in the 3-st GAGC layer. (c) Correlation map of the complete data. (d) Correlation map of incomplete data.

the information of incomplete hidden states is compressed into compact representations and then is recovered to the complete states. Fig. 8 (a) shows that only a fraction of the information is directed towards the projector, while different attention heads can provide varying levels of information density. Meanwhile, Fig. 8 (b) denotes that a small number of coordinates can reconstruct useful neural representations for subsequent imputation.

We further examine the singular value distribution of

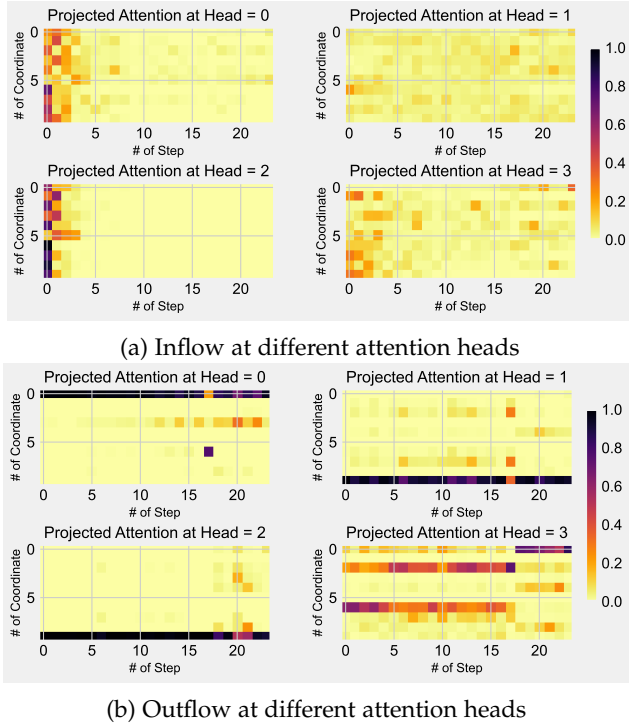


Fig. 8: Inflow and outflow of temporal information in the projected attention layer. The x-axis is the number of time steps, and the y-axis is the number of projected coordinates.

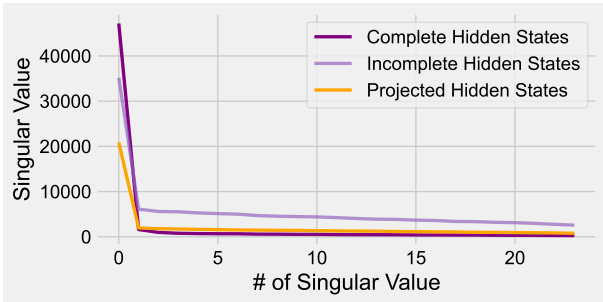


Fig. 9: Singular value distribution of different hidden representations in the temporal attention layer.

different hidden representations in the last temporal attention layer. As evidenced by Fig. 9, after flow through the projected attention layer, the hidden states have lower singular values than the incomplete inputs and are closer to the complete representations.

5 CONCLUSION

This paper demonstrates a knowledge-powered graph Transformer model termed *ImputeFormer* to address the missing spatiotemporal data imputation problem. By exploiting the low-rank and redundant nature of time series, we design projected temporal attention and global adaptive graph convolution to enhance the Transformer model. Additionally, a Fourier imputation loss is developed to serve as a structural inductive bias. The evaluation results indicate that *ImputeFormer* not only consistently achieves state-of-the-art imputation accuracy, but also exhibits high efficiency,

generalizability across other datasets, and interpretability of the results. Therefore, we believe that *ImputeFormer* has the potential to advance research on foundational models for general imputation tasks. Future work can adopt *ImputeFormer* to achieve time series forecasting with sparse historical observations.

ACKNOWLEDGMENTS

This research was sponsored by the National Natural Science Foundation of China (52125208), the Science and Technology Commission of Shanghai Municipality (No. 22dz1203200), and the National Natural Science Foundation of China's Young Scientists Fund (52302413).

REFERENCES

- [1] Y. Duan, Y. Lv, Y.-L. Liu, and F.-Y. Wang, "An efficient realization of deep learning for traffic data imputation," *Transportation research part C: emerging technologies*, vol. 72, pp. 168–181, 2016.
- [2] X. Chen, Z. He, and L. Sun, "A bayesian tensor decomposition approach for spatiotemporal traffic data imputation," *Transportation research part C: emerging technologies*, vol. 98, pp. 73–84, 2019.
- [3] Y. Chen, Y. Lv, and F.-Y. Wang, "Traffic flow imputation using parallel data and generative adversarial networks," *IEEE Transactions on Intelligent Transportation Systems*, vol. 21, no. 4, pp. 1624–1630, 2019.
- [4] C. Chen, K. Petty, A. Skabardonis, P. Varaiya, and Z. Jia, "Freeway performance measurement system: mining loop detector data," *Transportation Research Record*, vol. 1748, no. 1, pp. 96–102, 2001.
- [5] X. Chen, J. Yang, and L. Sun, "A nonconvex low-rank tensor completion model for spatiotemporal traffic data imputation," *Transportation Research Part C: Emerging Technologies*, vol. 117, p. 102673, 2020.
- [6] H. Li, M. Li, X. Lin, F. He, and Y. Wang, "A spatiotemporal approach for traffic data imputation with complicated missing patterns," *Transportation research part C: emerging technologies*, vol. 119, p. 102730, 2020.
- [7] Y. Ye, S. Zhang, and J. J. Yu, "Spatial-temporal traffic data imputation via graph attention convolutional network," in *International Conference on Artificial Neural Networks*. Springer, 2021, pp. 241–252.
- [8] T. Nie, G. Qin, and J. Sun, "Truncated tensor Schatten p-norm based approach for spatiotemporal traffic data imputation with complicated missing patterns," *Transportation research part C: emerging technologies*, vol. 141, p. 103737, 2022.
- [9] T. Nie, G. Qin, Y. Wang, and J. Sun, "Correlating sparse sensing for large-scale traffic speed estimation: A laplacian-enhanced low-rank tensor kriging approach," *Transportation Research Part C: Emerging Technologies*, vol. 152, p. 104190, 2023.
- [10] X. Wang, Y. Wu, D. Zhuang, and L. Sun, "Low-rank hankel tensor completion for traffic speed estimation," *IEEE Transactions on Intelligent Transportation Systems*, vol. 24, no. 5, pp. 4862–4871, 2023.
- [11] X. Chen, M. Lei, N. Saunier, and L. Sun, "Low-rank autoregressive tensor completion for spatiotemporal traffic data imputation," *IEEE Transactions on Intelligent Transportation Systems*, vol. 23, no. 8, pp. 12301–12310, 2021.
- [12] S. Liu, X. Li, G. Cong, Y. Chen, and Y. Jiang, "Multivariate time-series imputation with disentangled temporal representations," in *The Eleventh International Conference on Learning Representations*, 2022.
- [13] W. Ma and G. H. Chen, "Missing not at random in matrix completion: The effectiveness of estimating missingness probabilities under a low nuclear norm assumption," *Advances in neural information processing systems*, vol. 32, 2019.
- [14] W. Cao, D. Wang, J. Li, H. Zhou, L. Li, and Y. Li, "Brits: Bidirectional recurrent imputation for time series," *Advances in neural information processing systems*, vol. 31, 2018.
- [15] Z. Che, S. Purushotham, K. Cho, D. Sontag, and Y. Liu, "Recurrent neural networks for multivariate time series with missing values," *Scientific reports*, vol. 8, no. 1, p. 6085, 2018.

- [16] A. Cini, I. Marisca, and C. Alippi, "Filling the gaps: Multivariate time series imputation by graph neural networks," *arXiv preprint arXiv:2108.00298*, 2021.
- [17] W. Du, D. Côté, and Y. Liu, "Saits: Self-attention-based imputation for time series," *Expert Systems with Applications*, vol. 219, p. 119619, 2023.
- [18] I. Marisca, A. Cini, and C. Alippi, "Learning to reconstruct missing data from spatiotemporal graphs with sparse observations," *Advances in Neural Information Processing Systems*, vol. 35, pp. 32 069–32 082, 2022.
- [19] M. Liu, H. Huang, H. Feng, L. Sun, B. Du, and Y. Fu, "Pristi: A conditional diffusion framework for spatiotemporal imputation," *arXiv preprint arXiv:2302.09746*, 2023.
- [20] J. Ma, Z. Shou, A. Zareian, H. Mansour, A. Vetro, and S.-F. Chang, "Cds: cross-dimensional self-attention for multivariate, geo-tagged time series imputation," *arXiv preprint arXiv:1905.09904*, 2019.
- [21] X. Chen, C. Zhang, X.-L. Zhao, N. Saunier, and L. Sun, "Nonstationary temporal matrix factorization for multivariate time series forecasting," *arXiv preprint arXiv:2203.10651*, 2022.
- [22] A. Das, W. Kong, R. Sen, and Y. Zhou, "A decoder-only foundation model for time-series forecasting," *arXiv preprint arXiv:2310.10688*, 2023.
- [23] A. Garza and M. Mergenthaler-Canseco, "Timegpt-1," *arXiv preprint arXiv:2310.03589*, 2023.
- [24] S. Van Buuren and K. Groothuis-Oudshoorn, "mice: Multivariate imputation by chained equations in r," *Journal of statistical software*, vol. 45, pp. 1–67, 2011.
- [25] X. Yi, Y. Zheng, J. Zhang, and T. Li, "St-mvl: filling missing values in geo-sensory time series data," in *Proceedings of the 25th International Joint Conference on Artificial Intelligence*, 2016.
- [26] H.-F. Yu, N. Rao, and I. S. Dhillon, "Temporal regularized matrix factorization for high-dimensional time series prediction," *Advances in neural information processing systems*, vol. 29, 2016.
- [27] X. Chen and L. Sun, "Bayesian temporal factorization for multidimensional time series prediction," *IEEE Transactions on Pattern Analysis and Machine Intelligence*, vol. 44, no. 9, pp. 4659–4673, 2021.
- [28] M. Jin, H. Y. Koh, Q. Wen, D. Zambon, C. Alippi, G. I. Webb, I. King, and S. Pan, "A survey on graph neural networks for time series: Forecasting, classification, imputation, and anomaly detection," *arXiv preprint arXiv:2307.03759*, 2023.
- [29] Y. Luo, X. Cai, Y. Zhang, J. Xu et al., "Multivariate time series imputation with generative adversarial networks," *Advances in neural information processing systems*, vol. 31, 2018.
- [30] J. Yoon, J. Jordon, and M. Schaar, "Gain: Missing data imputation using generative adversarial nets," in *International conference on machine learning*. PMLR, 2018, pp. 5689–5698.
- [31] Y. Luo, Y. Zhang, X. Cai, and X. Yuan, "E2gan: End-to-end generative adversarial network for multivariate time series imputation," in *Proceedings of the 28th international joint conference on artificial intelligence*. AAAI Press Palo Alto, CA, USA, 2019, pp. 3094–3100.
- [32] Y. Liu, R. Yu, S. Zheng, E. Zhan, and Y. Yue, "Naomi: Non-autoregressive multi-resolution sequence imputation," *Advances in neural information processing systems*, vol. 32, 2019.
- [33] Y. Tashiro, J. Song, Y. Song, and S. Ermon, "Csdi: Conditional score-based diffusion models for probabilistic time series imputation," *Advances in Neural Information Processing Systems*, vol. 34, pp. 24 804–24 816, 2021.
- [34] S. Shan, Y. Li, and J. B. Oliva, "Nrtsi: Non-recurrent time series imputation," in *ICASSP 2023-2023 IEEE International Conference on Acoustics, Speech and Signal Processing (ICASSP)*. IEEE, 2023, pp. 1–5.
- [35] Y. Liang, Z. Zhao, and L. Sun, "Memory-augmented dynamic graph convolution networks for traffic data imputation with diverse missing patterns," *Transportation Research Part C: Emerging Technologies*, vol. 143, p. 103826, 2022.
- [36] Y. Wu, D. Zhuang, A. Labbe, and L. Sun, "Inductive graph neural networks for spatiotemporal kriging," in *Proceedings of the AAAI Conference on Artificial Intelligence*, vol. 35, no. 5, 2021, pp. 4478–4485.
- [37] W. Liang, Y. Li, K. Xie, D. Zhang, K.-C. Li, A. Souri, and K. Li, "Spatial-temporal aware inductive graph neural network for c-ts data recovery," *IEEE Transactions on Intelligent Transportation Systems*, 2022.
- [38] T. Nie, G. Qin, Y. Wang, and J. Sun, "Towards better traffic volume estimation: Jointly addressing the underdetermination and nonequilibrium problems with correlation-adaptive gnns," *Transportation Research Part C: Emerging Technologies*, vol. 157, p. 104402, 2023.
- [39] A. Vaswani, N. Shazeer, N. Parmar, J. Uszkoreit, L. Jones, A. N. Gomez, L. Kaiser, and I. Polosukhin, "Attention is all you need," in *Advances in Neural Information Processing Systems*, 2017, pp. 5998–6008.
- [40] J. Dong, H. Wu, H. Zhang, L. Zhang, J. Wang, and M. Long, "Simmtm: A simple pre-training framework for masked time-series modeling," *arXiv preprint arXiv:2302.00861*, 2023.
- [41] Y. Nie, N. H. Nguyen, P. Sinthong, and J. Kalagnanam, "A time series is worth 64 words: Long-term forecasting with transformers," *arXiv preprint arXiv:2211.14730*, 2022.
- [42] Z. Li, Z. Rao, L. Pan, P. Wang, and Z. Xu, "Ti-mae: Self-supervised masked time series autoencoders," *arXiv preprint arXiv:2301.08871*, 2023.
- [43] A. Dosovitskiy, L. Beyer, A. Kolesnikov, D. Weissenborn, X. Zhai, T. Unterthiner, M. Dehghani, M. Minderer, G. Heigold, S. Gelly et al., "An image is worth 16x16 words: Transformers for image recognition at scale," *arXiv preprint arXiv:2010.11929*, 2020.
- [44] J. Gao and B. Ribeiro, "On the equivalence between temporal and static equivariant graph representations," in *International Conference on Machine Learning*. PMLR, 2022, pp. 7052–7076.
- [45] Z. Shao, Z. Zhang, F. Wang, W. Wei, and Y. Xu, "Spatial-temporal identity: A simple yet effective baseline for multivariate time series forecasting," in *Proceedings of the 31st ACM International Conference on Information & Knowledge Management*, 2022, pp. 4454–4458.
- [46] T. Nie, G. Qin, Y. Wang, and J. Sun, "Nexus sine qua non: Essentially connected neural networks for spatial-temporal forecasting of multivariate time series," *arXiv preprint arXiv:2307.01482*, 2023.
- [47] A. Zeng, M. Chen, L. Zhang, and Q. Xu, "Are transformers effective for time series forecasting?" *arXiv preprint arXiv:2205.13504*, 2022.
- [48] Z. Wu, S. Pan, G. Long, J. Jiang, X. Chang, and C. Zhang, "Connecting the dots: Multivariate time series forecasting with graph neural networks," in *Proceedings of the 26th ACM SIGKDD International Conference on Knowledge Discovery and Data Mining*. New York, NY, USA: Association for Computing Machinery, 2020, p. 753–763.
- [49] A. Cini, I. Marisca, D. Zambon, and C. Alippi, "Taming local effects in graph-based spatiotemporal forecasting," *arXiv preprint arXiv:2302.04071*, 2023.
- [50] H. Liu, Z. Dong, R. Jiang, J. Deng, J. Deng, Q. Chen, and X. Song, "Spatio-temporal adaptive embedding makes vanilla transformer sota for traffic forecasting," in *Proceedings of the 32nd ACM International Conference on Information and Knowledge Management*, 2023, pp. 4125–4129.
- [51] Y. Zhang and J. Yan, "Crossformer: Transformer utilizing cross-dimension dependency for multivariate time series forecasting," in *The Eleventh International Conference on Learning Representations*, 2022.
- [52] J. Liu, P. Musialski, P. Wonka, and J. Ye, "Tensor completion for estimating missing values in visual data," *IEEE transactions on pattern analysis and machine intelligence*, vol. 35, no. 1, pp. 208–220, 2012.
- [53] T. G. Kolda and B. W. Bader, "Tensor decompositions and applications," *SIAM review*, vol. 51, no. 3, pp. 455–500, 2009.
- [54] Z. Wu, S. Pan, G. Long, J. Jiang, and C. Zhang, "Graph wavenet for deep spatial-temporal graph modeling," *arXiv preprint arXiv:1906.00121*, 2019.
- [55] Z. Shao, Z. Zhang, F. Wang, and Y. Xu, "Pre-training enhanced spatial-temporal graph neural network for multivariate time series forecasting," in *Proceedings of the 28th ACM SIGKDD Conference on Knowledge Discovery and Data Mining*, 2022, pp. 1567–1577.
- [56] G. Liu and W. Zhang, "Recovery of future data via convolution nuclear norm minimization," *IEEE Transactions on Information Theory*, vol. 69, no. 1, pp. 650–665, 2022.
- [57] H. Wu, T. Hu, Y. Liu, H. Zhou, J. Wang, and M. Long, "Timesnet: Temporal 2d-variation modeling for general time series analysis," *arXiv preprint arXiv:2210.02186*, 2022.
- [58] C. for Energy Regulation (CER), "CER Smart Metering Project - Electricity Customer Behaviour Trial, 2009-2010," [dataset] 1st Edition. Irish Social Science Data Archive. SN: 0012-00. <https://www.ucd.ie/issda/data/commissionforenergyregulationcer/>, 2012.
- [59] Y. Li, R. Yu, C. Shahabi, and Y. Liu, "Diffusion convolutional recurrent neural network: Data-driven traffic forecasting," *arXiv preprint arXiv:1707.01926*, 2017.